

Article

Estimation of Tendon Force Distribution in Prestressed Concrete Girders Using Smart Strand

Keunhee Cho * , Sung Tae Kim, Jeong-Rae Cho and Young-Hwan Park

Structural Engineering Research Institute, Korea Institute of Civil Engineering and Building Technology, 283, Goyangdae-Ro, Ilsanseo-Gu, Goyang-Si 10223, Gyeonggi-Do, Korea; esper009@kict.re.kr (S.T.K.); chojr@kict.re.kr (J.-R.C.); yhpark@kict.re.kr (Y.-H.P.)

* Correspondence: kcho@kict.re.kr; Tel.: +82-31-910-0132

Received: 25 October 2017; Accepted: 13 December 2017; Published: 19 December 2017

Abstract: The recently developed smart strand offers the possibility of measuring the prestress force of the tendon from jacking and all along its service life. In the present study, a method estimating the force distribution in all the tendons of a prestressed concrete (PSC) girder installed with one smart strand is proposed. The force distribution in the prestressed tendons is formulated by the friction and the anchorage slip, and is obtained through an optimization process with respect to the compatibility conditions and equilibrium of the forces in the section of the PSC girder. The validation of the proposed method through a numerical example and experiment shows that it can be used to estimate the force developed in the tendon.

Keywords: smart strand; strand; tendon; prestress; force distribution; optical fiber sensor

1. Introduction

The prestress force in a prestressed concrete (PSC) structure is mostly introduced by means of steel strand. Since such steel strands are the most important member of the PSC structure, their rupture is likely to degrade structural health. It is noteworthy that, despite its primary role, it has been challenging to directly measure the prestress distribution within the structure prior to the development of the smart strand [1–5]. The prestress force was estimated indirectly by a formula calculating the loss of prestress using the hydraulic pressure measured externally at the jacked end of the structure and the change in the length of the tendon before and after prestressing [6–8].

The recent development of the smart strand, which can measure the strain of the strand all along its service from jacking, offers the possibility of accurately measuring the distribution of the prestress force in the tendon. The smart strand can be fabricated by attaching the optical fiber between the neighboring helical wires [4,5] or by replacing the steel core wire with a core wire in which the optical fiber is embedded. In such case, the core wire is made by inserting the optical fiber inside a hollow steel tube [2] or by pultruding a carbon fiber reinforced polymer (CFRP) rod [1] or a glass fiber reinforced polymer (GFRP) rod [3] with the optical fiber monolithically. Moreover, the strain can be measured at the locations at which the fiber Bragg grating (FBG) is engraved in the optical fiber [1,2] or all along the optical fiber using the Brillouin wave [9]. Figure 1 presents a typical configuration of the smart strand in which the steel core wire is replaced by a core wire with sensing function.

As shown in Figure 2, the PSC girder is generally prestressed by several tendons. Each tendon experiences some loss in prestress force due to the friction and the anchorage slip during the prestressing process. This results to the occurrence of discrepancy between the prestress forces developed outside and inside the structure. Moreover, the prestress force in a previously jacked tendon diminishes due to the shrinkage of the concrete structure generated by the subsequent jacking of the other tendons. Since there was no way to measure the force in the tendon before the development

of the smart strand, these losses of the prestress force were estimated by an indirect method [6]. However, the appearance of the smart strand opens up the possibility of measuring the change in the prestress force in the tendon all along the jacking process, thus directly computing the loss of the prestress force.

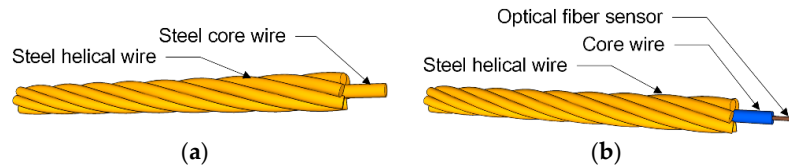


Figure 1. Shape and composition of conventional and smart strands: (a) Conventional strand; (b) Smart strand.

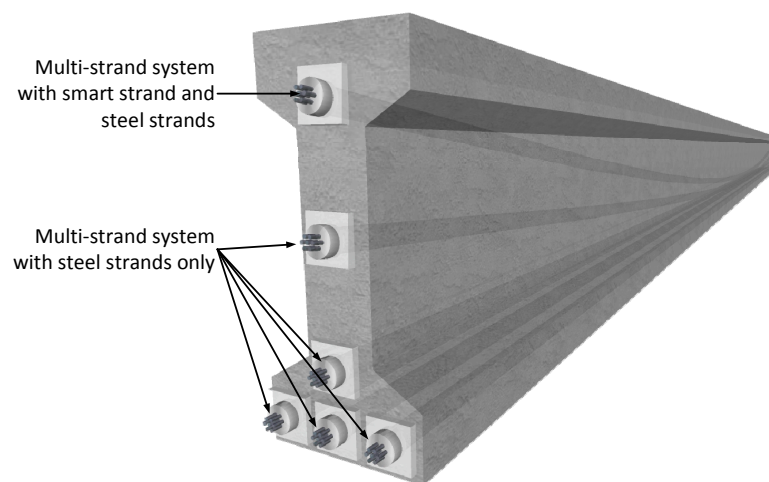


Figure 2. Prestressed concrete (PSC) girder with multiple tendons.

Ideally, the smart strand should be installed in each tendon to directly measure the change of prestress force in the tendons. However, in practice, the smart strand is installed only in a limited number of the tendons because of the higher cost of the smart strand compared to the conventional strand. Accordingly, this study intends to propose a method for estimating the prestress force distribution in all the tendons of the PSC girder when only one smart strand is installed as shown in Figure 2.

2. Formulations

The formulation is done in the case where the smart strand is installed in the first tendon to be prestressed in the PSC girder with multiple tendons. This condition that the tendon installed with the smart strand must be prestressed first is essential for knowing the force distribution in all the tendons equipping the PSC girder. The present formulation can be applied through slight adjustment to the case where several smart strands are installed.

The prestress forces developed by the individual strands in a tendon differ to each other at the ends of the girder due to the braiding of the strands and the difference in their initial lengths [10–12]. This situation leads the prestress forces of the individual strands to also differ to each other inside the tendon itself. Consequently, the prestress force distribution in an individual strand resembles the prestress force distribution curve considering the friction but does not coincide exactly with it. However, the force distribution of the tendon consisting of bundles of these strands

fits with the prestress force distribution curve considering the friction by the force equilibrium. Therefore, the prestress force of the jacked tendon can be expressed as follows [7,8].

$$F_{ij}^{kp} = F_i^{kp} \exp(-\mu\alpha_{ij} - \kappa l_{ij}) \tag{1}$$

where μ and κ are respectively the curvature friction coefficient and the wobble friction coefficient; α_{ij} and κ_{ij} are respectively the changes in curvature and arclength in the j th section of the i th tendon; and F_i^{kp} and F_{ij}^{kp} are respectively the prestress force in the anchor of the i th tendon and the prestress force in the j th section at the k th jacking stage. The values of α_{ij} and κ_{ij} can be obtained from the profile of the tendon. The value of F_i^{kp} is also known since it is the jacking force applied during prestressing. Accordingly, the unknowns in the prestress force distribution of the tendon are μ and κ of which values, once determined, will allow the computation of the prestress force (F_{ij}^{kp}) in each section of the tendon.

The wedge is inserted after jacking. In this process, the anchorage slip occurs between the wedge and anchorage head. This anchorage slip provokes the change in the prestress force of the tendon at the jacked end, which can be expressed as follows [7,8].

$$F_{ij}^{ks} = F_i^{ks} (F_i^{kp}, \mu, \kappa, \Delta) \tag{2}$$

where Δ is the anchorage slip.

Since the tendon including the smart strand is prestressed first in this study, $k = 1$ and $i = 1$. Equations (1) and (2) can thus be rewritten as follows for the tendon with the smart strand.

$$F_{1j}^{1p} = F_1^{1p} \exp(-\mu\alpha_{1j} - \kappa l_{1j}) \tag{3}$$

$$F_{1j}^{1s} = F_1^{1s} (F_1^{1p}, \mu, \kappa, \Delta) \tag{4}$$

Dividing the prestress forces obtained from Equations (3) and (4) by the area (A_{p1}) and the elastic modulus (E_{p1}) of the tendon gives the strains (ϵ_{1j}^{1p} , ϵ_{1j}^{1s}). The elastic moduli of the conventional and smart strands composing the tendon are presented in the studies of Mattock [13] and Cho et al. [14].

After prestressing of the first tendon including the smart strand, the strain developed in each section of the concrete girder experiences changes due to the prestressing of the subsequent tendon. This also leads the prestress force of the previously prestressed tendon to change. Such changes in the strain must satisfy the following force equilibrium in each section.

$$\sum \Delta F = F_{ij}^t \cos \theta_{ij} + \sum_{i=1}^{k-1} E_{pi} A_{pi} \Delta \epsilon_{ij}^t \cos \theta_{ij} + \int_{A_j} E_c \Delta \epsilon_{c,j}^t dA = 0 \tag{5}$$

$$\sum \Delta M_z = F_{ij}^t \cos \theta_{ij} y_{ij} + \sum_{i=1}^{k-1} E_{pi} A_{pi} \Delta \epsilon_{ij}^t \cos \theta_{ij} y_{ij} + \int_{A_j} E_c \Delta \epsilon_{c,j}^t y_j dA = 0 \tag{6}$$

$$\sum \Delta M_y = F_{ij}^t \cos \theta_{ij} z_{ij} + \sum_{i=1}^{k-1} E_{pi} A_{pi} \Delta \epsilon_{ij}^t \cos \theta_{ij} z_{ij} + \int_{A_j} E_c \Delta \epsilon_{c,j}^t z_j dA = 0 \tag{7}$$

where t denotes the prestressing stage ($t = 2p, 2s, 3p, 3s, \dots$); F_{ij}^t is the prestress force of the tendon prestressed in each stage and can be obtained by means of Equations (1) and (2); $\Delta \epsilon_{c,j}^t (= \epsilon_{c,j}^t - \epsilon_{c,j}^{t-1})$ is the change in the strain of concrete occurring in the current stage; and, $\Delta \epsilon_{ij}^t (= \epsilon_{ij}^t - \epsilon_{ij}^{t-1})$ is the strain change experienced in the previously prestressed tendon at the current stage.

Assuming that a plane section of the concrete structure before deformation remains plane after deformation, the strain change ($\Delta \epsilon_{c,j}^t$) per prestressing stage in the concrete section can be expressed as follows.

$$\Delta\epsilon_{c,j}^t = \Delta\epsilon_{co,j}^t - y_j\Delta\kappa_{cz,j}^t + z_j\Delta\kappa_{cy,j}^t \tag{8}$$

where $\Delta\epsilon_{co,j}^t$, $\Delta\kappa_{cz,j}^t$ and $\Delta\kappa_{cy,j}^t$ respectively denote the strain change in the neutral axis of the j th section at the t th prestressing stage, and the curvature changes with respect to the z -axis and y -axis (Figure 3); y_j and z_j respectively represent the distances from the neutral axis of the section in the y -direction and z -direction.

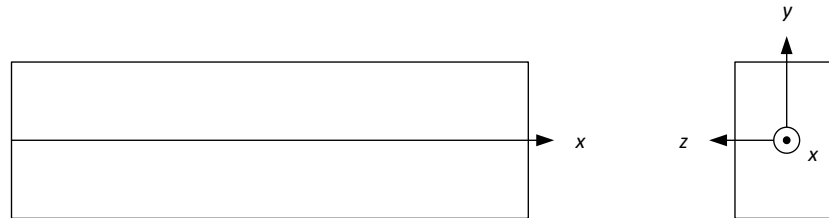


Figure 3. Coordinate system in the girder.

The integrated terms related to concrete in Equations (5)–(7) are arranged in Appendix A.

Moreover, if we assume that the prestressed tendon and concrete behave monolithically, the strain increment of the prestressed tendon can be expressed as follows using the strain of concrete.

$$\Delta\epsilon_{ij}^t = \Delta\epsilon_{co,j}^t - y_{ij}\Delta\kappa_{cz,j}^t + z_{ij}\Delta\kappa_{cy,j}^t \tag{9}$$

The unknowns in Equations (3)–(7) can be subdivided into the variables that keep constant values at each prestressing stage and those whose values vary. The variables that remain constant at each prestressing stage are μ , κ , Δ for the tendon and E_c for concrete. The variables with varying values at each prestressing stage are $\Delta\epsilon_{co,j}^t$, $\Delta\kappa_{cz,j}^t$, and $\Delta\kappa_{cy,j}^t$ for the deformation of concrete in each section. Among them, the unknowns representing the deformation of concrete can be obtained by the equilibrium of the forces given in Equations (5)–(7). Consequently, the problem of evaluating the tendon prestress force in the PSC girder is transformed to a problem searching for the curvature friction coefficient and wobble friction coefficient of the tendon, the anchorage slip, and the elastic modulus of concrete.

Solving Equations (5)–(7) for each section and at every prestressing stage provides then the strain state of the tendons. Among these so-obtained strains, an optimization problem can be formulated so as to minimize the difference between the strain increment ($\Delta\epsilon_{1j}^t$) of the tendon including the smart strand and the strain increment ($\Delta\epsilon_{1j,exp}^t$) measured by the smart strand. Equation (10) formulates the optimization problem which, once solved, will allow the remaining four other unknowns to be obtained.

$$\text{Minimize } \sum_t \sum_{j=1}^m \| \Delta\epsilon_{1j}^t - \Delta\epsilon_{1j,exp}^t \| \tag{10}$$

Each prestressing stage is subdivided into a substage (kp) in which the tendon is tensioned by the hydraulic jack, and another substage (ks) in which the wedge is fixed in the anchor head. The anchorage slip cannot be obtained in substage- kp because this substage is related only to the curvature friction coefficient, the wobble friction coefficient and the elastic modulus. Besides, all the unknowns can be obtained in substage- ks because this substage relates not only the curvature friction coefficient, the wobble friction coefficient, and the elastic modulus but also the anchorage slip. Accordingly, Equation (10) must consider the anchoring stage in order to obtain the anchorage slip.

Substituting the curvature friction coefficient, wobble friction coefficient, anchorage slip and elastic modulus obtained through this optimization process in Equations (1) and (2) enables us to find the strain distribution in the tendons at the prestressing stage and anchoring stage. The further strain

increment caused by additional prestressing can be obtained using Equation (9). The final tendon strain distribution can thus be described by summing them up until the last prestressing stage.

3. Numerical Verification

3.1. Without Variation

Figure 4 presents the example adopted to verify numerically the formulation process described in Section 2. The 20-m-long PSC girder (width of 0.6 m, height of 2.0 m) is equipped with three 12-strand tendons. The prestress force of each tendon is 2476 kN, and prestressing is performed sequentially downward from the tendon at the top (tendon #1). The smart strand is installed in tendon #1 and the strain is measured at seven points.

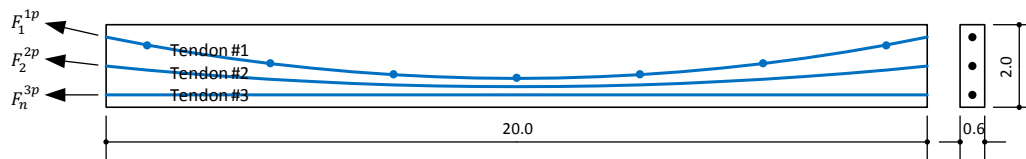


Figure 4. Example PSC girder for the verification of the proposed method (unit: m).

The proposed optimization method is performed considering the analysis cases listed in Table 1 for the girder shown in Figure 4. Figure 5 compares the tendon prestress forces for each of these analysis cases. The dots for tendon #1 indicate the measured values used as input during the optimization in Equation (10). The dots of tendons #2 and #3 represent the values obtained by finite element analysis for comparison and are not used in the optimization. The lines of each tendon plot the prestress forces obtained through optimization and are seen to be in good agreement with the measured or analytical values. Moreover, similar values are produced for the curvature friction coefficient, wobble friction coefficient, anchorage slip, and elastic modulus in each analysis case.

Table 1. Analysis cases for the verification example.

Case	Curvature Friction Coefficient	Wobble Friction Coefficient	Working Stroke of Anchorage	Elastic Modulus
Case A	0.2/rad	0.002/m	6 mm	33,979.6 MPa
Case B	0.2/rad	0.001/m	3 mm	30,000.0 MPa

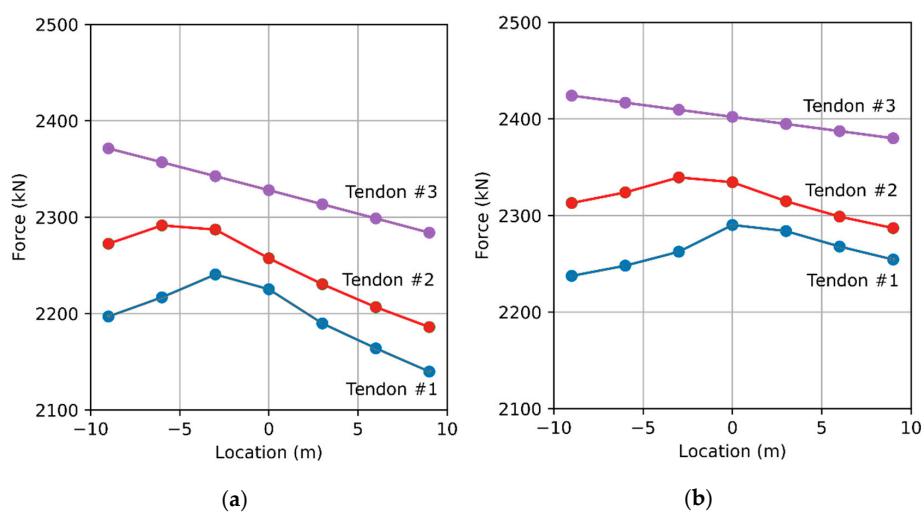


Figure 5. Comparison of tendon prestress force distributions per analysis case: (a) Case A; (b) Case B.

3.2. With Variation

Figure 5 corresponds to the ideal case where the prestress force measured by the smart strand coincides with the average prestress force of the tendon. However, Cho et al. [10] reported that, in reality, the prestress forces developed in the strands of the tendon differ to each other due to the braiding of the strands and that the prestress force distribution of the strands inside the tendon follows a normal distribution $N(f_{mean}, \sigma_f^2)$ where f_{mean} is the average prestress force of the tendon and σ_f is the standard deviation among the prestress forces.

$$\sigma_f = 0.019f_{mean} + 2.286 \text{ [kN]} \tag{11}$$

Consequently, the strain measured in the smart strand will also exhibit a pattern different to the ideal case. Need is thus to verify if the proposed method would provide an accurate estimation of the tendon force in such a non-ideal case. To that goal, assume the following expression for the strain measured by the smart strand.

$$\epsilon_{1j,exp}^{1p} = \frac{F_1^{1p} \exp(-\mu\alpha_{1j} - \kappa l_{1j})}{E_p A_p} + var \tag{12}$$

where var follows the normal distribution $N(\epsilon_{mean}, \sigma_\epsilon^2)$. The strain σ_ϵ can be obtained by dividing Equation (11) by the elastic modulus and area of the strand.

Optimization is then performed by applying the variation expressed by Equation (12) in the strain measured by the smart strand for the analysis case A. This optimization was carried out on 10 variations and the results are arranged in Table 2. The average values for each of the optimization variables show minimal error compared to the original system. In addition, the normalized error of the smart strand exhibits an average of about 2.9% and indicates the feasibility of the proposed method.

Figure 6 plots the strains measured by the smart strand together with the corresponding optimized strains for the variations with the smallest error, largest error and median error. Even if the measured strain profiles are very different to the ideal case, the tendon strain distribution resulting from the optimization appears to be very close to the ideal case. For the worst level of correspondence in Figure 6c, the error reaches only 3.6% at the location with the largest difference. Consequently, the method proposed in this study appears to be sufficiently applicable even in the case where the strain measured by the smart strand exhibits a different distribution profile due to the braiding of the strands.

Table 2. Optimization results for variations where the strain measured by the smart strand shows definite fluctuation.

Variation	Curvature Friction Coefficient (/rad)	Wobble Friction Coefficient (/m)	Working Stroke of Anchorage (mm)	Elastic Modulus (MPa)	Normalized Strain Error (%)
1	0.21	0.0020	6.0	33,943.9	1.0
2	0.19	0.0020	6.5	33,926.2	1.2
3	0.20	0.0020	6.6	33,896.1	1.6
4	0.17	0.0020	6.3	34,001.2	1.7
5	0.16	0.0019	7.2	33,922.2	2.6
6	0.22	0.0021	6.7	33,836.8	2.7
7	0.16	0.0019	6.1	34,057.1	2.8
8	0.26	0.0021	6.1	33,842.9	4.0
9	0.24	0.0021	6.7	33,784.2	4.1
10	0.12	0.0018	5.2	34,291.5	7.3
Average	0.19	0.002	6.3	33,950.2	2.9

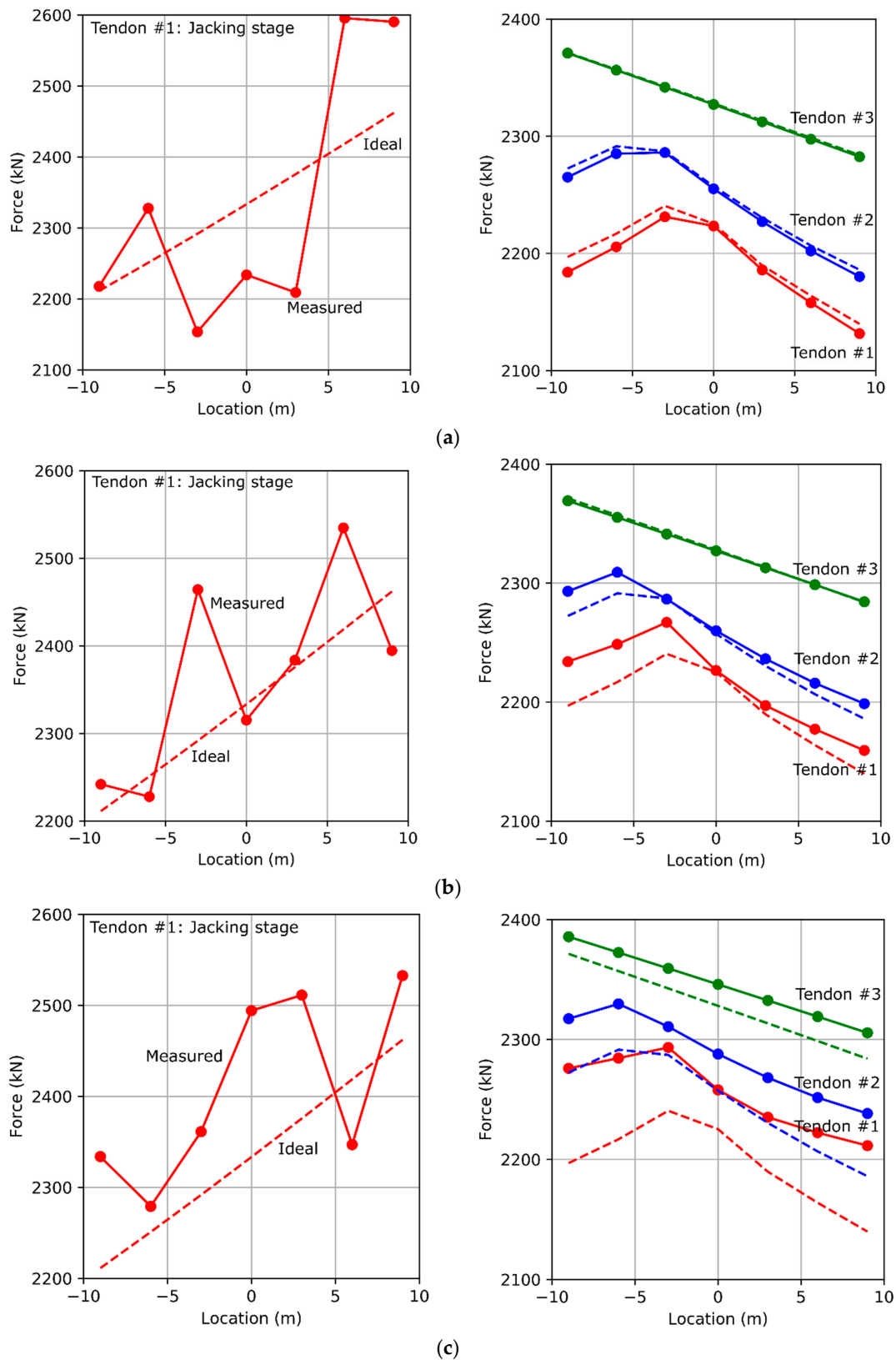


Figure 6. Comparison of prestress force distribution in cases where the strain measured by the smart strand shows definite fluctuation: (a) Variation #1: the smallest error; (b) Variation #7: the median error; (c) Variation #10: the largest error.

4. Experimental Validation and Discussions

The validity of the proposed method is verified experimentally as shown in Figure 7. The shape and size of the specimen are those of the girder adopted in the numerical analysis (Figure 4). The girder specimen is prestressed by three 12-strand tendons. The prestress force is 2109 kN in Tendon #1, 2045 kN in Tendon #2, and 2032 kN in Tendon #3. Jacking is done sequentially from Tendon #1 to Tendon #2 to Tendon #3. Tendon #1 and Tendon #2 are equipped smart strands having 7 FBGs, and Tendon #3 is installed with a smart strand having 5 FBGs.

Figure 8 plots the strains measured by the smart strands at each jacking stage. The strain is seen to decrease as much as the position becomes farther from the jacked end because of the friction within the tendon. In addition, the strain reduces at the jacked end due to the anchorage slip that occurred after setting. However, the measured strain does not fit exactly with the prestress force distribution predicted by the formula considering the friction due to the intertwisting of the strands inside the tendon.

Optimization was conducted by the proposed method using the values measured by the smart strand of Tendon #1. The results provided a curvature friction coefficient of 0.123/rad, a wobble friction coefficient of 0.0037/m, an anchorage slip of 4.65 mm, and a concrete elastic modulus of 25.2 GPa.

The strain distribution in each tendon could then be obtained based upon the optimization results. Figure 9 compares the measured prestress force distributions with the optimized ones from the start to the end of the jacking process. In the graphs, the gray lines represent the 95% confidence interval for the prestress force distribution of each strand. These lines were obtained from the average prestress force of the tendon resulting from optimization and standard deviation calculated by Equation (11).

The optimization results are seen to resemble the measured values but to not be in perfect coincidence. This can be attributed to the fact that the prestress force of each individual strand in the tendon is normally distributed and then the measured values of the smart strands is not necessarily identical to the average values of each tendon. This explains the apparent difference between the experimental values and the optimized average values. Moreover, the optimized value can have a certain level of error in the determination due to fluctuation of the measured value, as can be seen from the numerical verification. However, most of the values measured by the smart strands fall within the 95% confidence interval obtained from the optimized average prestress force. This proves that the proposed method can be applied even in the case where the measured value is not the average prestress force and indicates that the method can be used to estimate the prestress force distribution in the tendon.



Figure 7. Shape of specimen and jacking process.

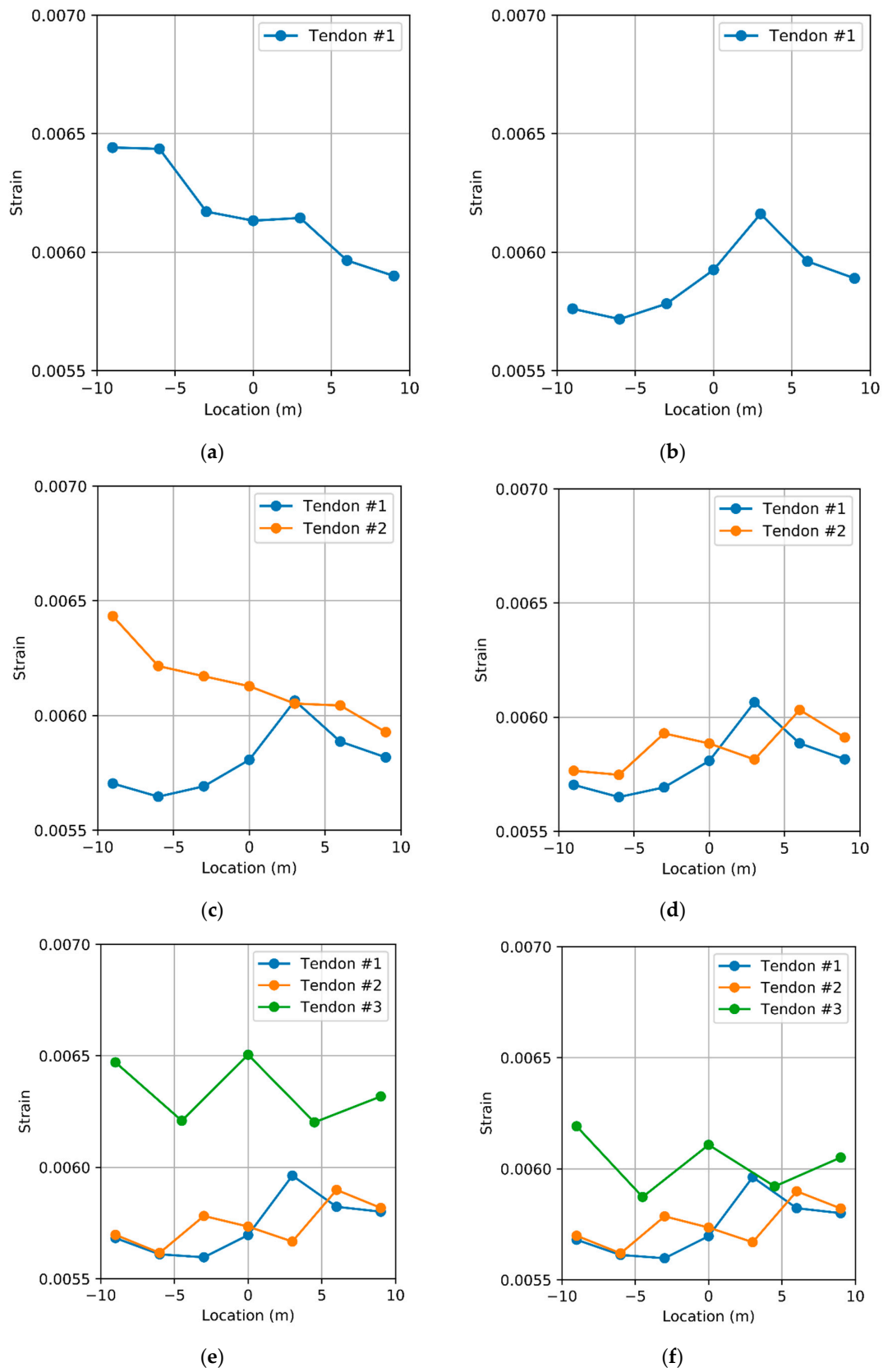


Figure 8. Strains measured by smart strands at each jacking stage: (a) Jacking of Tendon #1; (b) Setting of Tendon #1; (c) Jacking of Tendon #2; (d) Setting of Tendon #2; (e) Jacking of Tendon #3; (f) Setting of Tendon #3.

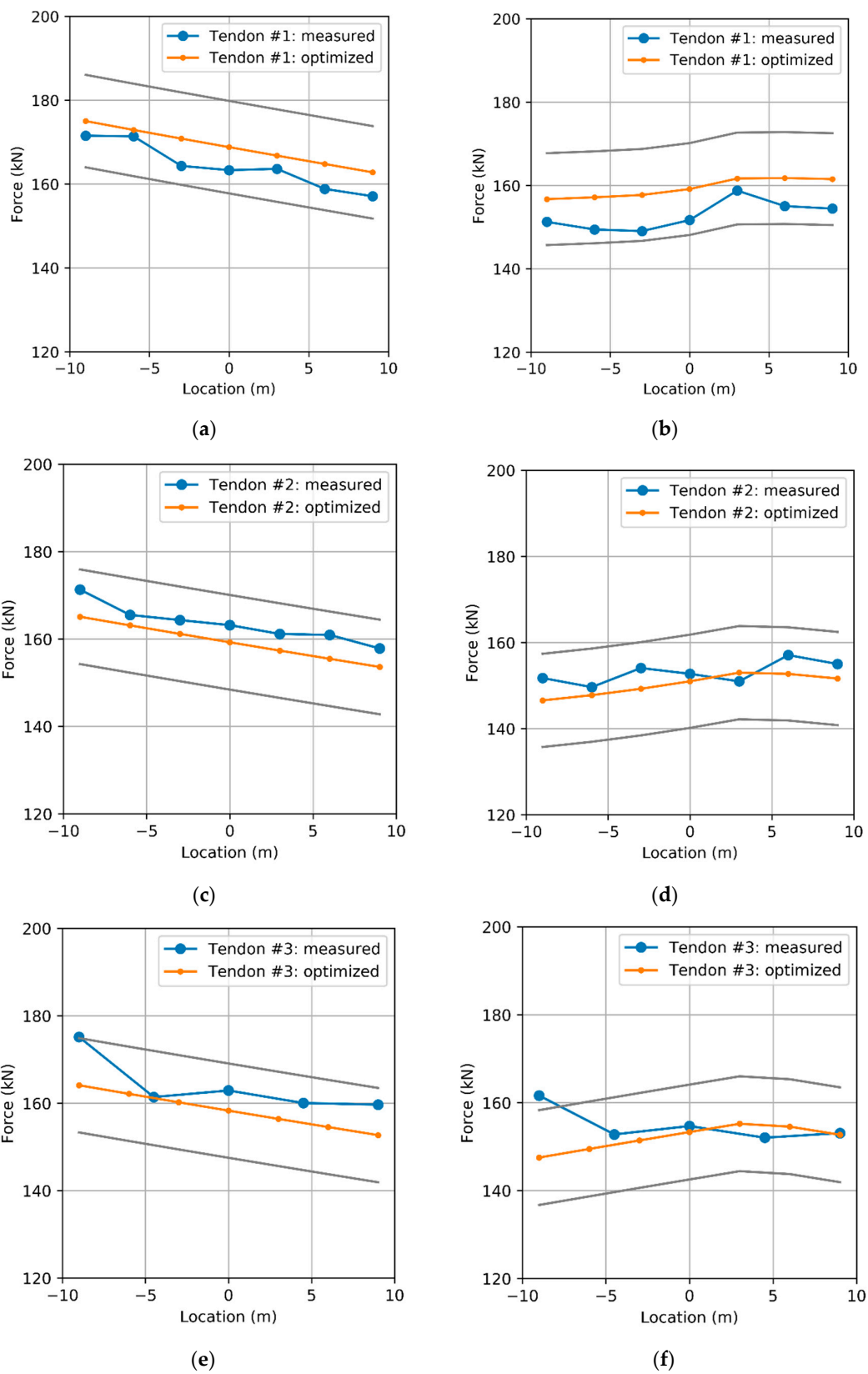


Figure 9. Comparison between experiment and optimization per jacking stage (gray lines represent 95% confidence interval): (a) Tendon #1: Jacking of Tendon #1; (b) Tendon #1: Setting of Tendon #3; (c) Tendon #2: Jacking of Tendon #2; (d) Tendon #2: Setting of Tendon #3; (e) Tendon #3: Jacking of Tendon #3; (f) Tendon #3: Setting of Tendon #3.

However, as shown in Section 3.2, the accuracy degrades when the measured strains diverge significantly from the average. Further study shall investigate the relation between the extent by which the measured strains diverge from the average and the accuracy of the proposed method. The prestress force varies continuously not only during jacking but also all along the service life of the structure, and influences the behavior of the structure [15,16]. Consequently, there is also need for a method estimating the change of the prestress force during jacking as well as with respect to time.

5. Conclusions

This study proposed a method estimating the final prestress force distribution in individual tendons of a PSC girder using the smart strand. This method expresses the tendon prestress force distribution in terms of parameters related to the friction and the anchorage slip and, correlates it to the compatibility and force equilibrium conditions in the PSC girder section at the sensing locations of the smart strand. The validity of the proposed method was verified numerically and experimentally. The numerical verification dealt with the cases where the strain measured by the smart strand agreed or disagreed with the prestress force distribution predicted by the formula considering the friction. The numerical results confirmed that the proposed method could estimate the prestress force distribution within a definite level of error. The experimental validation showed that the proposed method could provide prestress forces falling within 95% confidence interval even when the measured strain was not the average. Accordingly, the proposed method can be applied to estimate the prestress force distribution in the tendon. A method estimating the change in the prestress force not only during jacking but also all along the service life of the prestressed structure shall also be developed in the future.

Acknowledgments: This research was supported by a grant from a Strategic Research Project (Development of Smart Prestressing and Monitoring Technologies for Prestressed Concrete Bridges) funded by the Korea Institute of Construction and Building Technology.

Author Contributions: Keunhee Cho and Young-Hwan Park conceived the concept. Keunhee Cho, Jeong-Rae Cho and Sung Tae Kim established the formulation. Keunhee Cho and Jeong-Rae Cho verified the formulation. Keunhee Cho wrote the paper.

Conflicts of Interest: The authors declare no conflict of interest. The founding sponsors had no role in the design of the study; in the collection, analyses, or interpretation of data; in the writing of the manuscript, and in the decision to publish the results.

Appendix A

The integrated terms related to concrete forces in Equations (5)–(7) are arranged as follows by means of Equation (8).

$$\int_{A_j} E_c \Delta \epsilon_{c,j}^t dA = E_c A_{c,j} \Delta \epsilon_{c0,j}^t - E_c Q_{cz,j} \Delta \kappa_{cz,j}^t + E_c Q_{cy,j} \Delta \kappa_{cy,j}^t \tag{A1}$$

$$\int_{A_j} E_c \Delta \epsilon_{c,j}^t y_j dA = E_c Q_{cz,j} \Delta \epsilon_{c0,j}^t - E_c I_{cz,j} \Delta \kappa_{cz,j}^t + E_c I_{yz} \Delta \kappa_{cy,j}^t \tag{A2}$$

$$\int_{A_j} E_c \Delta \epsilon_{c,j}^t z_j dA = E_c Q_{cy,j} \Delta \epsilon_{c0,j}^t - E_c I_{yz} \Delta \kappa_{cz,j}^t + E_c I_{cy,j} \Delta \kappa_{cy,j}^t \tag{A3}$$

where $A_{c,j} = \int_{A_j} dA$; $Q_{cz,j} = \int_{A_j} y dA$; $Q_{cy,j} = \int_{A_j} z dA$; $I_{cz,j} = \int_{A_j} y^2 dA$; $I_{cy,j} = \int_{A_j} z^2 dA$; and, $I_{cyz,j} = \int_{A_j} yz dA$. When the cross-section is symmetric with respect to the y -axis, $Q_{cy,j} = I_{cyz,j} = 0$. When the cross-section is symmetric with respect to the z -axis, $Q_{cz,j} = I_{cyz,j} = 0$.

References

1. Kim, S.T.; Park, Y.; Park, S.Y.; Cho, K.; Cho, J.-R. A sensor-type pc strand with an embedded FBG sensor for monitoring prestress forces. *Sensors* **2015**, *15*, 1060–1070. [CrossRef] [PubMed]

2. Kim, J.-M.; Kim, C.-M.; Choi, S.-Y.; Lee, B.Y. Enhanced strain measurement range of an FBG sensor embedded in seven-wire steel strands. *Sensors* **2017**, *17*, 1654. [[CrossRef](#)] [[PubMed](#)]
3. Zhou, Z.; He, J.P.; Chen, G.D.; Ou, J.P. A smart steel strand for the evaluation of prestress loss distribution in post-tensioned concrete structures. *J. Intell. Mater. Syst. Struct.* **2009**, *20*, 1901–1912. [[CrossRef](#)]
4. Mckeeman, I.; Fusiek, G.; Perry, M.; Johnston, M.; Saafi, M.; Niewczas, P.; Walsh, M.; Khan, S. First-time demonstration of measuring concrete prestress levels with metal packaged fibre optic sensors. *Smart Mater. Struct.* **2016**, *25*, 095051. [[CrossRef](#)]
5. Perry, M.; Yan, Z.; Sun, Z.; Zhang, L.; Niewczas, P.; Johnston, M. High stress monitoring of prestressing tendons in nuclear concrete vessels using fibre-optic sensors. *Nucl. Eng. Des.* **2014**, *268*, 35–40. [[CrossRef](#)]
6. Preston, H.K.; Barker, J.M.; Boecker, J.R.H.C.; Dull, R.; Edwards, H.H.; Huang, T.; Iragorri, J.; Koretzky, H.P.; Kraemer, P.E.; Magura, D.D. Recommendations for estimating prestress losses. *PCI J.* **1975**, *20*, 43–75.
7. AASHTO. *Aashto LRFD Bridge Design Specifications*; AASHTO: Washington, DC, USA, 2014.
8. European Committee for Standardization. *Eurocode 2: Design of Concrete Structures—Part 1-1: General Rules and Rules for Buildings*; European Standards; European Committee for Standardization: London, UK, 2004.
9. Zhou, Z.; He, J.P.; Ou, J.P. Integrated optical fiber sensing system by combing large-scale distributed botda/r and localized FBGs. *Int. J. Distrib. Sens. Netw.* **2012**, *8*, 804394. [[CrossRef](#)]
10. Cho, K.; Cho, J.-R.; Kim, S.T.; Park, S.Y.; Kim, Y.-J.; Park, Y.-H. Estimation of prestress force distribution in multi-strand system of prestressed concrete structures using field data measured by electromagnetic sensor. *Sensors* **2016**, *16*, 1317. [[CrossRef](#)] [[PubMed](#)]
11. Chandoga, M.; Jarošević, A. Rehabilitation and monitored prestressing of corroded tendons. In Proceedings of the Fib Symposium: Structural Concrete and Time, La Plata, Argentina, 28–30 September 2005; pp. 1–8.
12. Cho, K.; Park, S.Y.; Cho, J.-R.; Kim, S.T.; Park, Y.-H. Estimation of prestress force distribution in the multi-strand system of prestressed concrete structures. *Sensors* **2015**, *15*, 14079–14092. [[CrossRef](#)] [[PubMed](#)]
13. Mattock, A.H. Flexural strength of prestressed concrete sections by programmable calculator. *PCI J.* **1979**, *24*, 32–54. [[CrossRef](#)]
14. Cho, K.; Kim, S.T.; Cho, J.-R.; Park, Y.-H. Analytical model of nonlinear stress-strain relation for a strand made of two materials. *Materials* **2017**, *10*, 1003. [[CrossRef](#)]
15. Noble, D.; Nogal, M.; O'Connor, A.; Pakrashi, V. The effect of prestress force magnitude and eccentricity on the natural bending frequencies of uncracked prestressed concrete beams. *J. Sound Vib.* **2016**, *365*, 22–44. [[CrossRef](#)]
16. Noble, D.; Nogal, M.; O'Connor, A.; Pakrashi, V. *The Effect of Post-Tensioning Force Magnitude and Eccentricity on the Natural Bending Frequency of Cracked Post-Tensioned Concrete Beams*; Journal of Physics: Conference Series; IOP Publishing: Bristol, UK, 2015; p. 012047.

